RESEARCH PAPER

CrossMark

Stiffness Degradation and Damping Ratio of Sand-Gravel Mixtures Under Saturated State

Meysam Bayat[1] · **Abbas Ghalandarzadeh**[1]

Abstract

The aim of this research was to explain the effects of gravel content using the intergrain state concept, relative density and confining pressure on G_{max}, G/G_{max}–γ and D–γ curves and the reference strain (γ_r). A total of 45 G–γ and D–γ curves derived from resonant column testing and cyclic triaxial testing along with S-wave velocity measurements obtained using the bender element technique were assessed. The test specimens were prepared with different gravel contents (0, 30, 50, 75 and 100%) under different relative densities (10, 30 and 60%) and mean effective confining pressures (100, 300 and 600 kPa). Comparison of the G_{max} results of the resonant column and bender element tests was also carried out. The desired excitation frequencies and ratios λ/D_{50} and d/λ (where λ is wavelength, d is transmission path length and D_{50} is average particle size) were determined based on the bender element tests results. The test results were used to evaluate the empirical equation for prediction of G_{max} and to develop a new prediction equation with which to estimate γ_r. The results of the tests were used to validate previous models and empirical curves.

Keyword Dynamic properties · Gravel content · Cyclic triaxial · Bender element · Resonant column

1 Introduction

The small-strain shear modulus (G_{max}) along with the normalized modulus degradation (G/G_{max}) and damping ratio increase (D) from small to large shear strains (γ) are necessary data for geotechnical seismic analyses. To evaluate the response of soil layers under different types of dynamic loading (such as impact, wind, vehicle loads, detonation and earthquake loading), an appropriate evaluation of the shear modulus and damping properties of the various soil layers is necessary and critical for the design of structures subjected to vibrations [1]. For this purpose, advanced laboratory testing techniques have been specifically developed to study the dynamic properties of soil. In this context, resonant column (RC) and cyclic triaxial (CT) tests were conducted under ASTM [2, 3]. There are several advantages of the bender element technique, namely its simplicity and ease of use;

however, no standard has been developed for this testing technique or to interpret the results obtained from BE tests. Nevertheless, BE testing has been used extensively by researchers in the laboratory to evaluate the dynamic properties of soil. As illustrated in Fig. 1, each apparatus can be used for a certain range of strains. In the current study, an advanced cyclic triaxial apparatus incorporating BEs, local displacement measurement and a RC apparatus have been used to measure stiffness and damping for a broad range of strain amplitudes.

Studies have shown that the most important parameters affecting the dynamic properties of soil are external parameters such as loading properties (stress–strain path, stress–strain amplitude, stress–strain rate and stress–strain duration) and material properties (soil type, grain size distribution curve, shape of soil grains and density) [5]. The most important factors that affect the shear modulus and damping ratio of granular soil are the amplitude of shear strain, effective confining pressure and relative density. Less important parameters are frequency of loading and degree of saturation [6]. Although many researchers have studied the factors affecting the G/G_{max}–γ and D–γ curves for clayey, silty and sandy soil [6–14], there is relatively little research

✉ Abbas Ghalandarzadeh
aghaland@ut.ac.ir

Meysam Bayat
bayat.m@ut.ac.ir

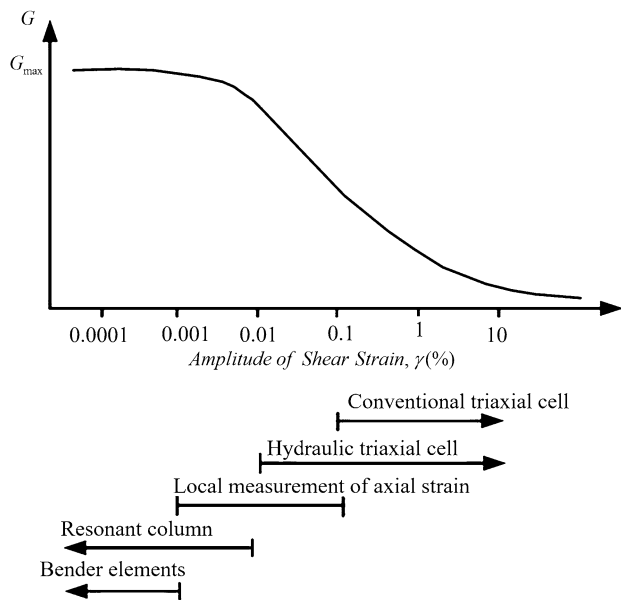1 School of Civil Engineering, College of Engineering, The University of Tehran, Tehran, Iran

Springer

Fig. 1 Variation of stiffness with strain measured with diffident laboratory tests after Atkinson et al. [4]

concerning the dynamic properties of sand-gravel mixtures [8, 15–18].

Hardin [15] studied the dynamic properties of granular soil using a free–free resonant column device. The results showed that the dynamic properties of gravelly soil are a function of void ratio, confining pressure and grain characteristics. Seed et al. [8] presented the results of cyclic triaxial tests on gravelly soil. Based on the results, they proposed a set of nonlinear shear modulus and damping ratio curves for sandy and gravelly soil. They also suggested the use of the D–γ curves for sandy and gravelly soil using damping curves suggested by Seed and Idriss [19] for sands. Lin et al. [17] used large-scale cyclic triaxial testing to study the dynamic properties of gravelly deposits. Their results show that gravel content has an important effect on the nonlinear behaviour of gravelly soil under large strains. The G/G_{max} of the specimens which contained 60 and 80% gravel increased at shear strains larger than 0.1%. This trend was not observed in specimens containing 20 and 40% gravel. Tanaka et al. [16] tested reconstituted gravelly soil and showed that effective confining pressure has an important effect on the nonlinear dynamic parameters of gravelly soil as well as on the nonlinear dynamic parameters of sandy soil. They concluded that gravelly soil behaved more linearly as the isotropic confining stress increases. Soil having a lower gravel content (GC = 25%) behaved slightly more linearly than soil having a higher gravel content (GC = 50%).

Despite these research efforts, the behaviour of granular material under seismic loading remains not fully understood and is currently the subject of interesting research.

Therefore, in the current study, shear strain amplitude, mean effective confining pressure, relative density and gravel content were selected as the controlled variables during the design of the experimental program.

The initial or maximum of shear modulus (G_0 or G_{max}) at shear strain levels of less than 0.001% is an important parameter in earthquake engineering and a variety of geotechnical design applications. It is possible to offer a functional relationship between shear modulus degradation versus strain level by using a reliable value of G_{max} along with completed stress–strain curves of the soil. G_{max} can be determined in the laboratory using an RC test or a BE installed on conventional test devices such as the triaxial apparatus. Gu and Yang [20] indicated that among various test methods for evaluation of G_{max}, the RC test is recognized as the most reliable. In the current study, the results of BE tests are evaluated by comparison with RC data.

Hardin and Black [21] showed that G_{max} depends primarily on the void ratio of the soil e and mean effective confining pressure σ'_m as:

$$G_{max} = Af(e)\left(\sigma'_m\right)^n, \tag{1}$$

where A and n are the model parameters that are, in turn, linked to grain size distribution characteristics and $f(e)$ is a void ratio function reflecting the effect of density [22].

The concept of reference strain, γ_r (a shear strain amplitude in which $G/G_{max} = 0.5$), is useful in comparisons of nonlinearity parameters. Seed et al. [8] indicated that the γ_r of gravelly soil (about 0.012%) is lower than that of sandy soil (about 0.036%). In the other words, gravelly soil behaves more nonlinearly than sandy soil when deformed under the same shear strain amplitude, which agrees with the results of Tanaka et al. [16]. Reference strain γ_r has been studied for different soils, but there has been a significant lack of information on the γ_r for sand-gravel mixtures thus far. In the current study, the γ_r of sand-gravel mixtures under various confining pressures and relative densities has been examined. This paper presents test data from BE, CT and RC tests on pure sand, pure gravel and sand-gravel mixtures. It summarizes the findings from an experimental program assessing the dynamic properties of the specimens at different relative densities tested under various confining pressures.

2 Testing Program and Materials

2.1 Materials

A series of tests were performed on specimens of Firoozkooh sand 161 and Metosak gravel under saturated conditions to investigate the influence of relative density, gravel content and mean confining pressure on the dynamic
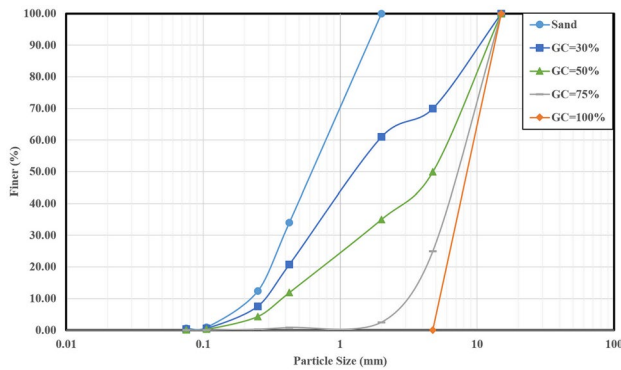
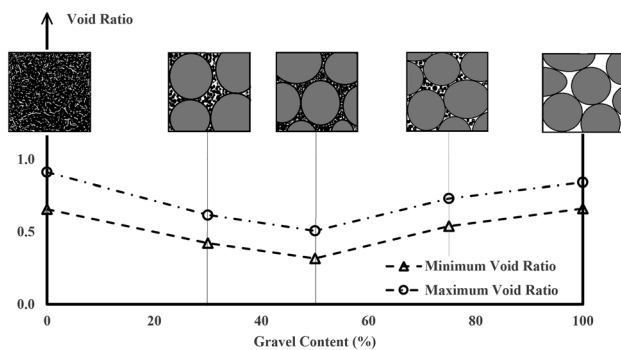**Fig. 2** Grain size distribution curves of the sand–gravel mixtures

Fig. 3 Maximum and minimum composite void ratios versus gravel content

properties. Firoozkooh sand 161 was chosen for testing because it has been well characterized in the literature and is a clean, uniformly-graded fine-sand with a silt content of less than 1%, which should enhance the reproduction of the specimens. Note that Firoozkooh sand 161 is classified as SP according to the USCS.

The Metosak gravel is a uniform gravel soil with a maximum particle size of less than 17 mm. The geotechnical properties of the sand-gravel mixtures were determined in the laboratory and the grain size distribution curves are shown in Fig. 2. Figure 3 shows the maximum and minimum void ratios (e_{max} and e_{min}) versus gravel content for the materials. The e_{max} and e_{min} values were obtained for the sand-gravel mixtures in accordance with ASTM [23, 24]. As shown in Fig. 3, the values of e_{max} and e_{min} declined significantly with an increase in gravel content from 0 to 50%. For gravel contents of 0–50%, it appeared that the gravel grains float in the sand matrix and there is little contact between the gravel grains. The values of e_{max} and e_{min} increased as the gravel content increased to more than 50% and contact between the gravel grains increased. The results of e_{max} and e_{min} are in good agreement with those of previous studies, such as Evans and Zhou [25]. On the other hand, the results

of e_{max} and e_{min} show that, it is impossible to compare the dynamic properties of composite specimens with different gravel contents using an identical void ratio. For this reason, in the current study, the effect of gravel content on the dynamic properties of the sand-gravel mixtures was investigated at given relative densities.

2.2 Specimen Preparation

Researchers have used several specimen reconstitution techniques in an element testing device. Previous studies indicate that the specimen reconstitution technique has important effect on the behaviour of soil [26]. One method of specimen preparation is the wet tamping technique, which has the advantage of easy control of soil density [27, 28]. In the present work, the wet tamping technique was used with a low initial water content and consideration of under-compaction of the lower layers during preparation [29, 30]. Details of the wet tamping technique can be found in Fakharian and Eghbali [31]. The same specimen preparation procedure was employed for both reconstituted specimens of RC and CT in split molds using the wet tamping technique.

During specimen preparation, dry gravel was mixed with dry sand at various weight ratios (0, 30, 50, 75 and 100%). According to ASTM [3], neither the length nor the diameter of the test specimen should be less than approximately 6 times the size of the largest particle intended for use. The specimens were compacted with a diameter equal to 100 mm, and a height/diameter relation close to 2. After specimen preparation and measurement of the diameter and height, full saturation is required to perform the RC and CT tests. For this purpose, the specimen were first subjected to a flow of CO_2 from the bottom to the top and were then saturated with de-aired water. The back pressure technique was used to ensure a saturated state. According to ASTM [32], the Skempton's B coefficient must be greater than 0.95 in the tests. Following saturation, the saturated soil specimens were isotopically consolidated under a given confining stress (σ_3). In the triaxial apparatus, after completion of the consolidation stage, a wave signal was generated using a signal wave generator in the transmitter bender element before cyclic loading.

3 Test Apparatuses and Testing Procedures

3.1 Cyclic Triaxial Test

The results of the cyclic triaxial tests were used to obtain the dynamic properties for medium-to-large shear strain amplitudes (10^{-4} to 10^{-2}). The procedure defined by ASTM [3] is usually used to identify the dynamic characteristics of soil by using hysteresis loops under cyclic loading. For

this purpose, constant cyclic shear stress loading started at a small amplitude and was gradually increased. Each stage of loading consisted of 40 loading cycles. Drainage was not allowed during each stage of loading, the excess pore water pressure generated during dynamic loading was dissipated before the next stage of loading. The tenth cycle hysteresis loops of loading in each stage was used to compute the dynamic properties.

The slope of a secant line that connects the extreme points on the hysteresis loop was denoted as shear modulus G. Damping ratio D is a measure of dissipated energy W_D versus elastic strain energy W_S and can be calculated as:

$$D = \frac{W_D}{4\pi W_S} = \frac{1}{2\pi} \times \frac{A_{loop}}{G\gamma^2}. \tag{2}$$

The cyclic triaxial tests were carried out according to ASTM [3] to evaluate the dynamic properties of the soil at a frequencies of 0.5 to 1.0 Hz, although ASTM [33] recommends a frequency variation between 0.1 and 2 Hz (with 1 Hz preferred). Previous research has suggested that an increase in frequency leads to an increase in the shear modulus of some soils [34]. Consequently, in the current study, all the cyclic triaxial tests were performed using a constant cyclic load with a sinusoidal wave at a constant frequency of 1 Hz and the first half cycle in compression. Estimations of the shear modulus and shear strain parameters could be obtained using Poisson's ratio, ν, which was taken as 0.5 for the saturated undrained condition [35].

Determination of soil dynamic parameters under small strains can be difficult in the laboratory because of the insufficient resolution and accuracy when measuring the load and displacement. In the other words, measuring the axial strain of a specimen outside the triaxial cell introduces significant error (bedding error and apparatus compliance) into the computation of strain, particularly in the small-strain range [36]. As shown in Fig. 4, two LVDTs were installed directly on the either side of the specimen without puncturing the surrounding rubber membrane to measure the relative local axial strain, which was calculated as the average of two LVDTs.

3.2 Bender Element Test

A pair of bender elements (a transmitter and receiver) was installed in the top cap and base pedestal of the triaxial apparatus to apply shear waves in the axial direction.

The most common methodologies for interpreting BE results are generally grouped into time-domain (TD) and in the frequency domain (FD) methods. The time domain method is the simplest to implement as far as computational capabilities; however, it can prove to be more difficult than the other methods due to the need for the user to manually

Fig. 4 Prepared specimen along with two LVDTs

decide which arrival to select. It is best performed by a researcher with experience at selecting the arrival time and with a knowledge of wave propagation principles as well as the mechanical behavior of the bender elements. Since the traces are time-averaged, the selection of the arrival time becomes even more unambiguous. Although the frequency domain method of selecting the arrival time reduces the user-bias associate with arrival selections, it still requires someone with expertise to perform post-processing verification of the experimental results. As opposed to the time domain method, which is continuously performed with the judgement of the user, thus readily identifying anomalous waveforms, the computer automated method of FD is more prone to overlooking such instanced that might greatly affect the subsequent outcome.

In the current study TD method has been used for interpreting BE results. In order to calculate the shear wave velocity (V_S), the time delay between the sender and receiver signals and the distance traveled is required. In the current study, the first major deflection on the received signal was used to determine the shear wave arrival time. Using the theory of shear wave propagation in an elastic body, the shear modulus was calculated from the measurement of the shear wave velocity and mass density of the soil ρ as:

$$G = \rho V_S^2. \tag{3}$$

3.3 Resonant Column Test

Because of the limitations associated with cyclic triaxial incorporation of BEs, resonant column testing is required to obtain the complete curves for G–γ and D–γ for a wide range

of strains. RC testing has become a standard in geotechnical engineering to study the small strain response of geomaterials commonly performed at frequencies above 30 Hz [2, 37]. In the current study, a free–free resonant column device was used in which the actuator was mounted on the top of the sample and the bottom was free to rotate. The free–free resonant frequency method is a simple approach used by many researchers to measure small-strain dynamic properties. Based on boundary condition of the RC apparatus and basic dynamic relations, the following relations have been obtained for the free–free RC apparatus:

$$G = \left(\frac{2\pi h f_R}{a} \right)^2 \times \rho, \tag{4}$$

$$a \tan (a) - \frac{J^2}{J_0 J_L} \times \frac{\tan (a)}{a} = \frac{J}{J_0} + \frac{J}{J_L}, \tag{5}$$

where h is the height of the specimen, ρ is the soil density and J, J_0 and J_L are the mass moment of the polar of the sample, the bottom part and the top part, respectively. From the relation of the RC apparatus, it can be concluded that α is a main RC parameter, relates to the geometry of the RC apparatus and is a function of the mass moment of the polar of the top and bottom parts of the RC. The value of J_0 and J_L for the RC apparatus were geometrically determined to be equal to 1.1819076 and 0.0688066 kg m^2, respectively.

In RC testing, the damping ratio can be determined by either the half-power bandwidth or free-vibration decay (FVD) methods. Ni [7] states that the half-power bandwidth method for measuring soil damping ratios is not suitable because serious error can be introduced into the damping ratios in nonlinear regions and that the free-vibration decay method should be used in this case. In order to minimize ambient noise, Hwang [38] and Stokoe et al. [9] suggest using three successive cycles for damping derivation with the assumption that material damping ratios do not change much within the shear strain variation of the first three cycles. In the current study, three successive cycles were implemented using the FVD method for damping derivation. Material damping for the FVD method can be calculated as:

$$D = \frac{1}{2\pi} \Delta, \tag{6}$$

where Δ_1 is the inclination of a log-linear plot of the shear strain amplitude versus the number of cycles.

4 Results and Discussion

4.1 Combined RC, BE and CT Equipment

A typical example of the combined results of the BE, RC and CT is presented in Fig. 5. This shows the results of the tests on the pure sand specimen at DR = 60% under a confining pressure of 600 kPa. BE was capable of detecting the shear modulus at very small strain amplitudes ($\gamma \leq 10^{-5}$). The values for the shear modulus and damping ratio were then extracted from the results of RC testing ($4 \times 10^{-6} < \gamma < 2 \times 10^{-4}$). Finally, the shear modulus and damping ratio in the medium to large strain amplitudes were obtained using CT testing ($2 \times 10^{-4} < \gamma$).

Researchers such as Huot and Vulliet [39] and Seed et al. [40] have indicated that the results will be more accurate if a load cell is placed inside the triaxial cell because this position avoids recording friction between the loading stem and triaxial cell. Preliminary testing of the triaxial device used indicated that the friction was very low, but, as the results showed, the small amount of friction affected the dynamic parameters at strain levels below 10^{-4}. Comparison of the results of RC testing with CT testing indicated that the measured shear modulus from the CT test was higher than that obtained from RC testing at a given strain below 10^{-4}. This difference resulted from placing the load cell outside the triaxial cell and using local LVDTs mounted at the surface of the specimen. In other words, although the axial strain was measured with high accuracy, even a small amount of friction could falsely increase the applied stress (or shear modulus), especially at shear strain levels below 10^{-4}.

4.2 Small-Strain Shear Modulus (G_{max})

Up to now, BE and RC tests have been widely utilized to determine the shear stiffness at shear strains of less than 10^{-5}, depending on the void ratio as well as the mean principal effective stress [41]. Relatively few publications could be
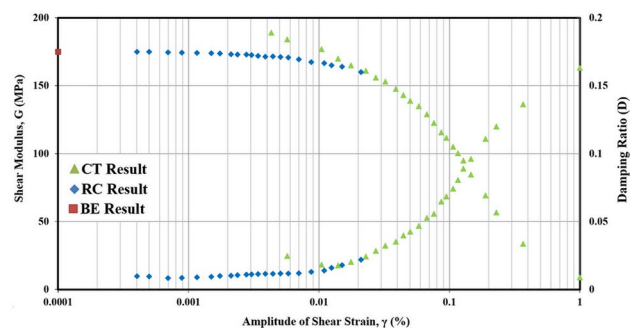
Fig. 5 A typical example of the combined results of the BE, RC and CT tests

found that compare the results of RC and BE testing. Dyvik and Madshus [42] and Fam et al. [43] and Hoyos et al. [44] found good agreement between the G_{max} values of sandy soil derived from the BE and RC techniques.

The size of the BE plays a more important role for a transmitter than a receiver. Flexibility is important for a receiver; it has an important effect on the strength of the signal acknowledged by a receiver. When the specimens were subjected to a high confining pressure, the motion of the BE was greatly impeded and could not vibrate at a strong enough intensity to produce a strong signal for the receiver to pick up. Increasing the size of the BE and its flexibility increased the intensity of the vibration of the BEs. When gravelly soil was used, two BEs of appropriate lengths (9 mm) were used.

A single sinusoidal pulse having a frequency of 6–25 kHz was used as the transmitted signal. The results show that the desired frequencies range depended on the gravel content. The desired excitation frequencies ranges are determined by comparing the test results of BE (Vs or G_0) with the results of RC tests. The desired excitation frequencies ranges based on gravel content are presented in Table 1. Outside of these ranges, very noisy received signals were found to be produced. The resonant frequency of the bender element is a very important parameter for near-field effect and travel time determinations. Although bender elements are not designed to create P-waves, they induce some weak P-waves due to compression effect of the vibration. The existence of near-field effect can mislead the travel time measurements. Recommended frequency ranges are more suitable for S-waves therefore formation of P-waves is minimized. Outside of these ranges, very noisy received signals were found to be produced and Finding the right answer is difficult. Near-field effect starts fading when the frequency range is limited down

to the ranges that presented in Table 1. Table 1 shows that the recommended ratio of λ/D_{50} (where λ is wavelength and D_{50} is average particle size) depends on the gravel content. For example, in order to avoid dispersion, the lower limit of λ/D_{50} of the pure sand and pure gravel specimens was 33 and 1, respectively. The results indicate that near-field effects can be minimized by using transmitted wave frequencies with a d/λ ratio (where d is transmission path length) higher than 3. This is in good agreement with the results of Leong et al. [45]. This restriction may be useful for avoiding overestimation of the shear wave velocity due to near-field effects. Table 1 also shows that the range of λ/D_{50} decreases as the gravel content increases.

Also in this section, the effects of gravel content, relative density and confining pressure on G_{max} are presented and G_{max-BE} (the value of G_{max} from BE data) is compared with G_{max-RC} (value of G_{max} from RC tests). Of the available methods for laboratory evaluation of shear modulus, the RC technique is recognized as the most reliable [20]. The results indicate that relative density had no significant effect on the difference between G_{max-BE} and G_{max-RC}; therefore, the average values of G_{max-BE} and G_{max-RC} of the specimens having different relative densities for a given confining pressure and gravel content were used to calculate G_{max-RC}/G_{max-BE} (Fig. 6). As shown, the G_{max} of the specimens with gravel contents of less than 75% from both methods were in good agreement, but G_{max-BE} for sand specimens containing 75 or 100% gravel were consistently lower than G_{max-RC}.

A significant difference between G_{max-BE} and G_{max-RC} was shown for the pure gravel specimens. This indicates that the BE test does not perform well in uniform coarse-grained soils, probably because of the path of the wave to reach the destination (Fig. 7). The wave generally follows a

Table 1 Summary of bender element test details

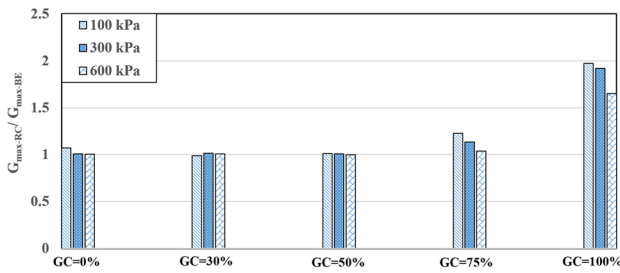| Gravel content	D_r	e	D_{50}	Desired frequency range (kHz)	λ/D_{50}	d/λ
0	10	0.890	0.607	6–15	82–33	3.7–9.1
	30	0.830				
	60	0.760				
30	10	0.597	1.15	6–8	48–36	3.1–4.1
	30	0.558				
	60	0.500				
50	10	0.488	4.75	6–10	13–8	3–5
	30	0.450				
	60	0.393				
75	10	0.711	7.07	8–10	5.4–4.3	4.7–5.8
	30	0.673				
	60	0.616				
100	10	0.822	8.3	20–25	1.3–1	15–18.6
	30	0.787				
	60	0.733				

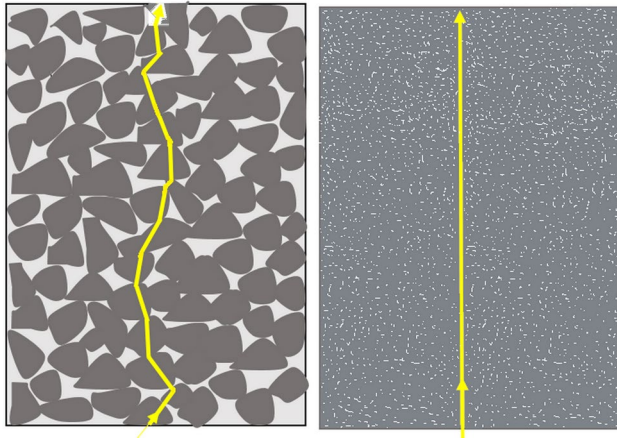**Fig. 6** Comparison between results of RC and BE tests

Fig. 7 Shear wave propagation in the pure gravel and pure sand specimens

shorter and more direct path in fine-grained soil specimens than in uniform coarse-grained soil specimens. The shear wave velocity and shear modulus of the specimens with high percentages of clean, well-rounded uniform gravel grains is much less than the corresponding values measured with RC tests.

The value of $G_{\text{max-RC}}$ versus relative density in terms of gravel content and confining pressure are presented in Fig. 8. As shown, G_{max} increased as the confining pressure or relative density increased [46, 47]. The value of $G_{\text{max-RC}}$ increased as the gravel content increased up to 50% and then decreased. Gravel specimens (GC = 100%) recorded greater values of $G_{\text{max-RC}}$ than specimens containing 75% gravel. The specimens containing 50% gravel recorded the highest $G_{\text{max-RC}}$ at a given relative density and confining pressure. Note that the specimens containing 50% gravel had the lowest void ratio when compared to other specimens at a given relative density.

The results of RC tests ($G_{\text{max-RC}}$) were used to evaluate the empirical equation in Eq. (1). The quality of the predictions of G_{max} are shown in Fig. 9. The predicted G_{max} values were plotted versus $G_{\text{max-RC}}$. Here, $f(e) = (2.17\_e)^2/(1+e)$ was adopted and the values for G_{max} and σ'_{m} in Eq. (1) are in kPa. Stress exponent (n) was used as a constant equal to 0.55 for all cases and A was considered to be a function of gravel content (Fig. 10). As shown in Fig. 9, most data points plotted close to the bisecting line.

4.3 Effect of Gravel Content on G/G_{max}–γ and D–γ Curves

The normalized modulus reduction and damping ratio curves of the specimens containing different gravel contents are presented in Fig. 11. Due to the large number of tests, only a few examples of the results are presented. As expected, the nonlinearity in the damping ratio curves resulted in an
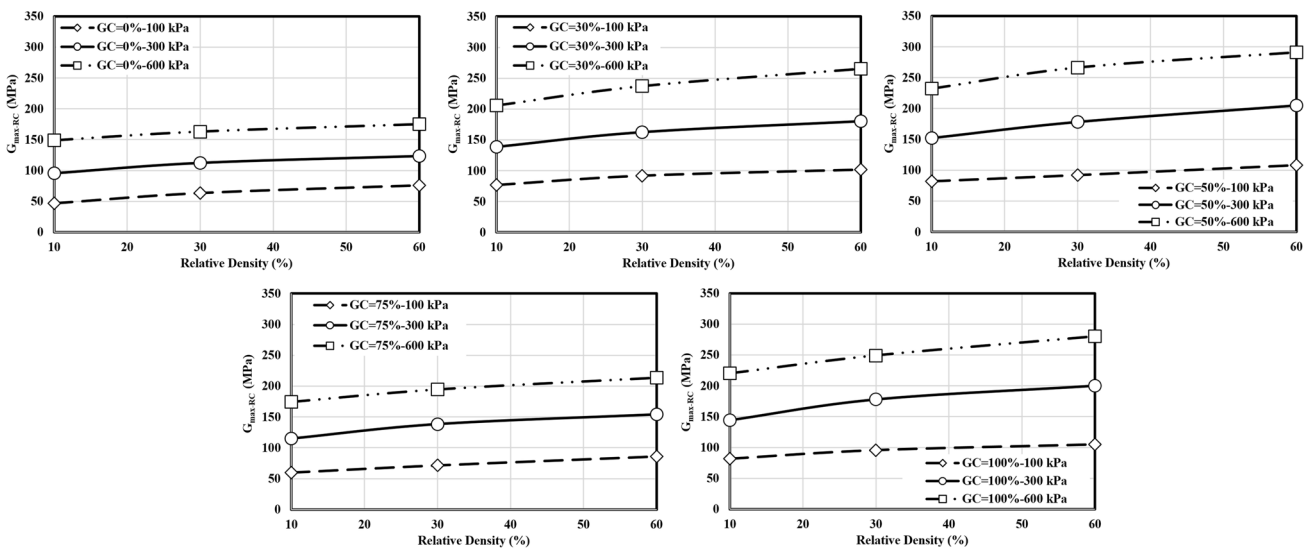

Fig. 8 Variation of $G_{\text{max-RC}}$ versus relative density
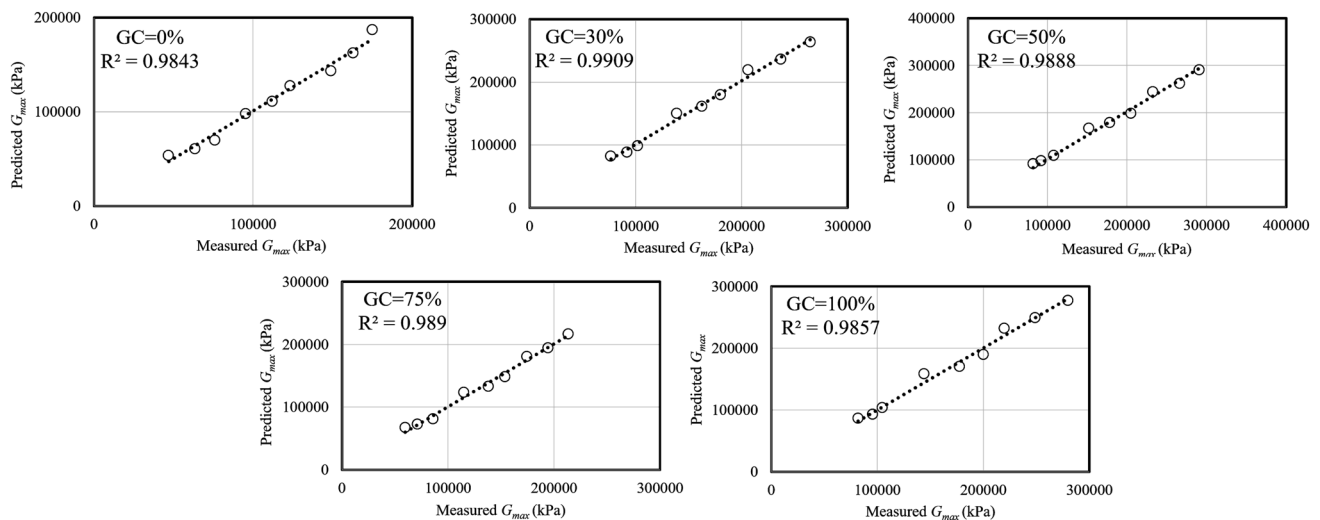
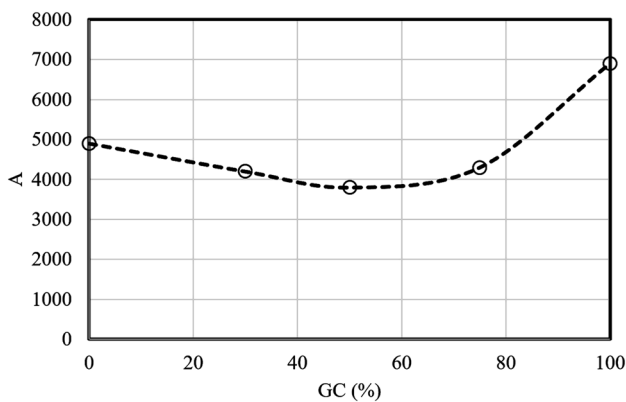**Fig. 9** Predicted versus measured values of G_{max} from RC tests

**Fig. 10** Variation of A parameter as a function of GC

increase in energy dissipation and in material damping ratio D with an increase in shear strain amplitude. As shown in the results, the pure sand specimen behaved slightly more linearly than the sand-gravel mixture specimens for a given confining pressure and relative density. In other words, the G/G_{max}–γ curves for the sand-gravel mixture specimens were much lower than that of the sand specimens for a given confining pressure and relative density. The results indicate that the specimens which contained 50% gravel are more nonlinear than other specimens when deformed to the same strain level at a given confining pressure and relative density. The increase in gravel content also slightly increased the damping ratio. The D–γ curves of the specimens with various gravel contents were close to each other, but the specimen containing 50% gravel exhibited the highest damping ratio at a given shear strain amplitude.

The G/G_{cs} ratios (ratio of the G of the sand-gravel mixture to the G of clean sand for a given shear strain level

under similar loading conditions) are good parameters to study the rate of degradation in the sand–gravel mixture stiffness. The G/G_{cs} ratios of the specimens are presented in Fig. 12. The results indicate that the rate of degradation in G/G_{cs} can be evaluated in three areas based on shear strain amplitude. The first is the degradation of the soil stiffness from very-small-to-small strains where the G/G_{cs} ratio is nearly constant or degradation rate of G/G_{cs} is very low. The small change in the degradation of the G/G_{cs} ratio at very small strain levels indicates that there was no sliding or rolling between gravel grains in the sand-gravel mixture specimens during cyclic loading. The second is the degradation of soil stiffness from small-to-medium strains where the rate of degradation of the G/G_{cs} ratio increased rapidly compared to the first region. In this region, sliding or rolling between gravel grains resulted in an increase in the degradation rate of the G/G_{cs} ratio. The highest degradation rate was for GC = 50%. The third area is the degradation of soil stiffness from medium-to-large strains with irregularities in the degradation ratio of G/G_{cs} due to the highly complex motion and rotation of the soil grains. As shown in Fig. 12, the lengths of these three areas depend on the gravel content, relative density and confining pressure.

The microstructures of the specimens with various gravel contents are shown in Fig. 13. The internal force chain network among particles and relative sliding between particles were affected by the microstructure. As shown in the results, most of the degradation of the normalized modulus curve and the high damping ratio was for specimens containing 50% gravel. This indicates that the part of the sand that is in contact with the surfaces of the gravel grains cause sliding and rolling of the gravel grains during cyclic loading (Fig. 14).

Fig. 11 Variation of G/G_{max} and D as a function of γ in terms of relative density and confining pressure
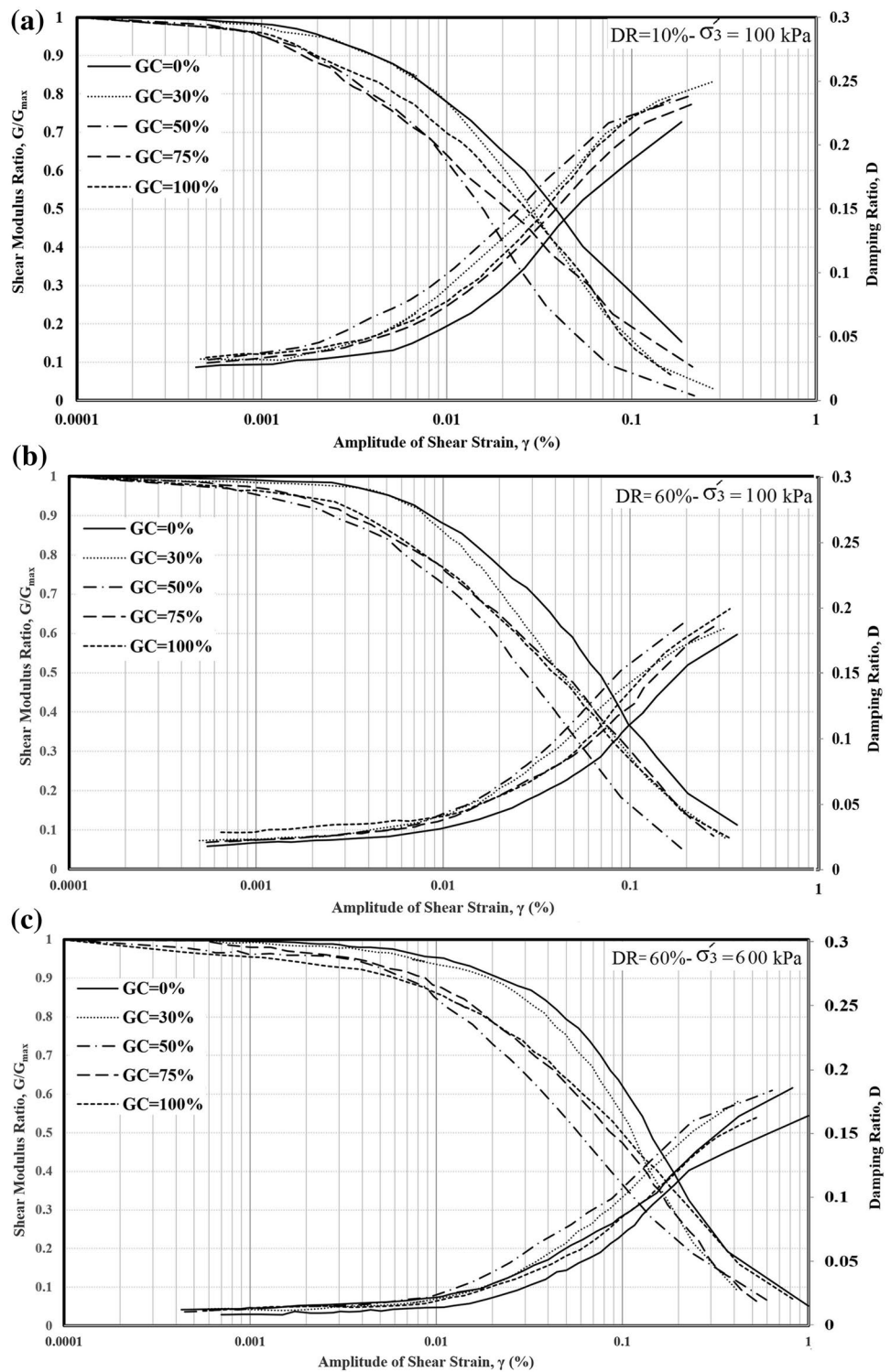
The effect of gravel content was assessed by comparing the strains occurring under compression and extension. Figure 15 shows the hysteresis loops for specimens at different gravel contents under a confining pressure of 600 kPa. As seen, shear strain developed relatively symmetrically in all specimens except those for which GC equalled 30 and 50%. The highest strength anisotropy was recorded for the specimen with a GC of 50% for which shear deformation under extension was considerably larger; this effect relates to anisotropy. A further decrease in the slope of the loops during the loading stage was evident in the specimen with a GC of 50%.

Fig. 12 Variation of G/G_{cs} as a function of γ in terms of relative density and confining pressure
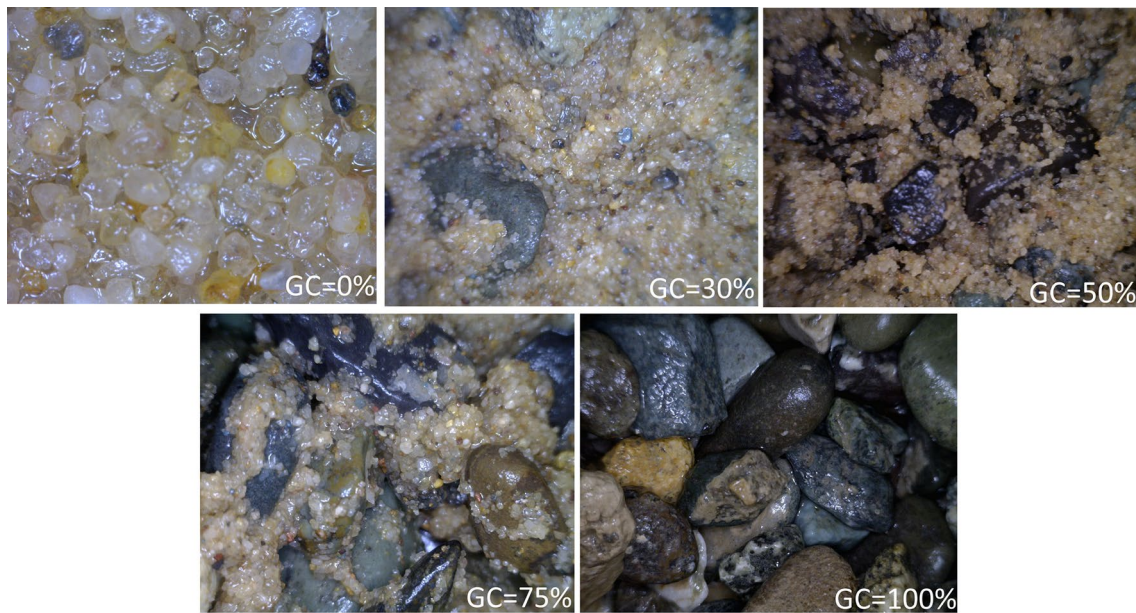

(a) DR=10%

(b) DR=30%

(c) DR=60%
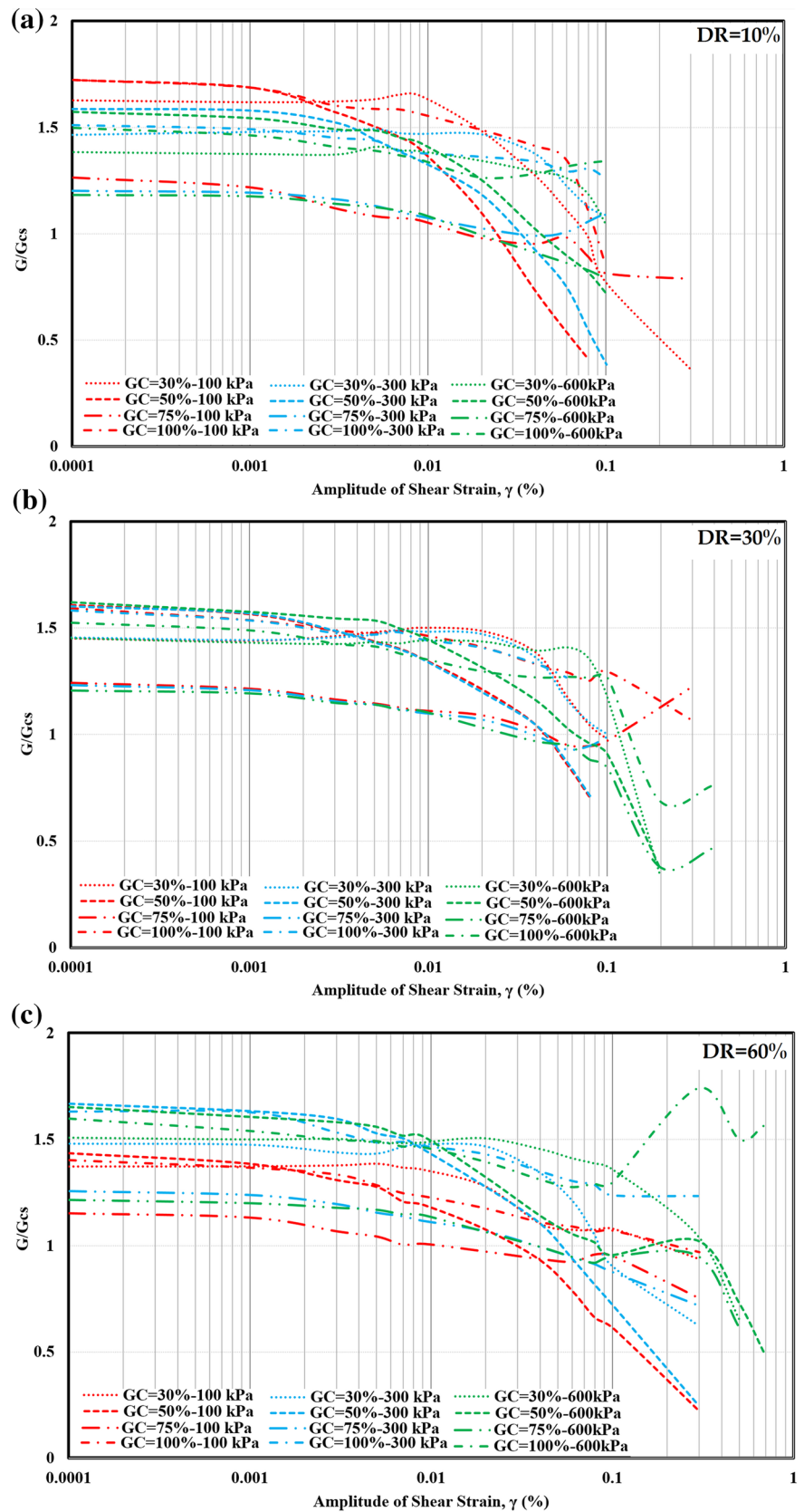
Fig. 13 The microstructures of the soil with various gravel content
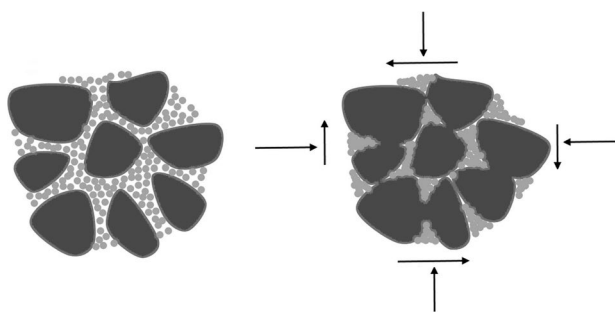

Fig. 14 Sliding and rolling between gravel grains in the specimens containing 50% gravel

The excess pore water pressure and shear strain amplitudes during cyclic loading are presented in Fig. 16. Cyclic loading in the undrained condition generated a pore pressure characterized by permanent pore-pressure component u_p and cyclic pore-pressure component u_{cy}.

Plastic deformation occurs when permanent deformation (γ_p) is developed during the loading process. As shown in the results, the residual excess pore-water pressure increased with repeated loading as did the cumulative plastic strain in the specimens with GC values of 100 and 75%. Energy dissipation by plastic deformation will occur when permanent deformation is developed in the loading process. As the
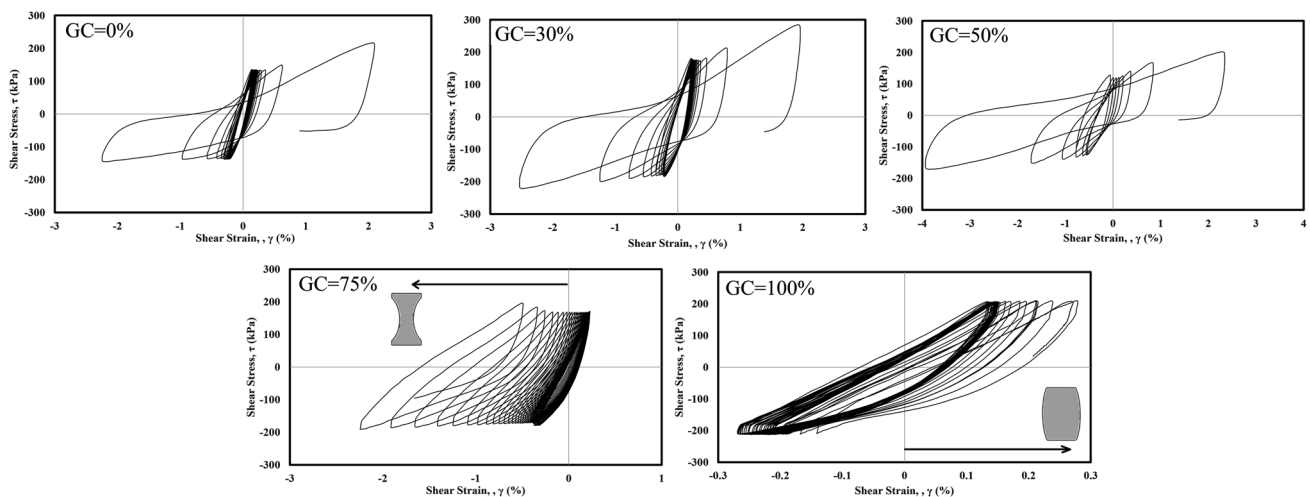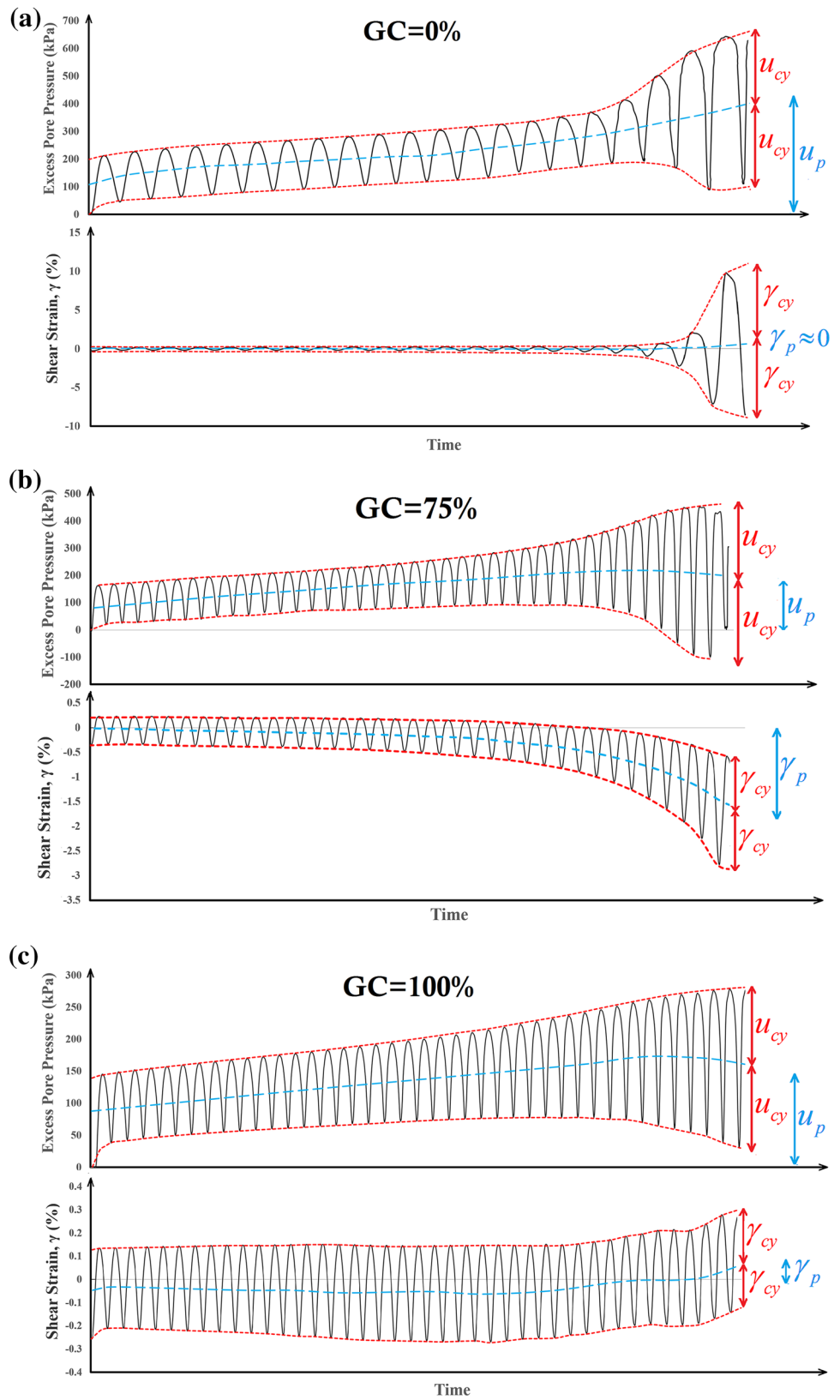

Fig. 15 Shear stress–strain hysteresis loops for the specimens with various gravel content at DR = 60% under confining pressure of 600 kPa

Fig. 16 Pore-pressure and shear strain as function of time under undrained cyclic loading

vibration amplitude increases, particles in granular systems temporarily lose contact or slide relative to each other. Permanent deformation or residual excess pore-water pressure of the specimens indicates that the particles slide and roll more freely over each other. The results show that the shear strain developed symmetrically without significant dominant permanent shear strain and large cyclic shear strain (γ_{cy}) at the end of loading stage in the specimens with GC values of 0, 30 and 50%. The shear strain was symmetrical and the permanent shear strain is positive (in compression mode) and negative (in extension mode), in the specimens with GC values of 100 and 75%, respectively.

4.4 Effects of Relative Density and Confining Pressure on G/G_{max}–γ and D–γ Curves

It is clear from comparison of Fig. 11a and b that the effect of relative density on the G/G_{max}–γ curves was significant at large shear strains. The effect of confining pressure can be investigated by comparing Fig. 11b and c. The results show that the damping ratio of the materials increased slightly as the relative density or confining pressure decreased. These findings are in good agreement with experimental results reported by RaviShankar [48].

The effect of confining pressure on the nonlinear behaviour and dynamic properties of sand-gravel specimens is easier to discuss in terms of reference threshold shear strain γ_r, which is simply the value of γ at $G/G_{max} = 0.5$ [49]. The variable γ_r is also regarded as a soil parameter for hyperbolic models of soils and is used to define the stiffness degradation curve [21, 49]. Figure 17 shows the reference strain versus relative density for various confining pressures. As shown, there was a slight increase in γ_r with an increase in relative density. Also, γ_r increased as the effective confining pressure increased, which is in good agreement with previous studies [6, 49].

The results show that relative density and confining pressure have more effect on the γ_r of the pure sand than on that of sand-gravel mixtures. The values of γ_r indicate that gravelly soil behaved more nonlinearly than sandy soil, which

agrees with the results of Tanaka et al. [16] and Seed et al. [8].

An equation similar to that of Eq. (1) for G_{max} can be used to prediction of γ_r:

$$\gamma_r = B f(e) \left(\sigma'_m\right)^n, \tag{7}$$

where B and n are the model parameters and σ'_m is the mean effective confining pressure (kPa).

The triaxial test results were used to evaluate the empirical constants in Eq. (7). The quality of the predictions of γ_r are shown in Fig. 18, where the predicted γ_r values are plotted versus the γ_r values obtained from testing. Here, $f(e) = (1.16 - e)^2/(1 + e)$ was adopted and stress exponent (n) was a constant value equal to 0.45 for all cases. As shown in Fig. 19, B is defined as a function of gravel content. Figure 18 shows that most data points plotted close to the bisecting line.

4.5 Comparison of Results With Previous Models and Empirical Curves

Hyperbolic models or empirical curves are widely used to describe the nonlinear behaviour of soil in geotechnical earthquake engineering [6, 11, 49]. Hardin and Drnevich [6] used hyperbolae to model shear stress–strain curves as:
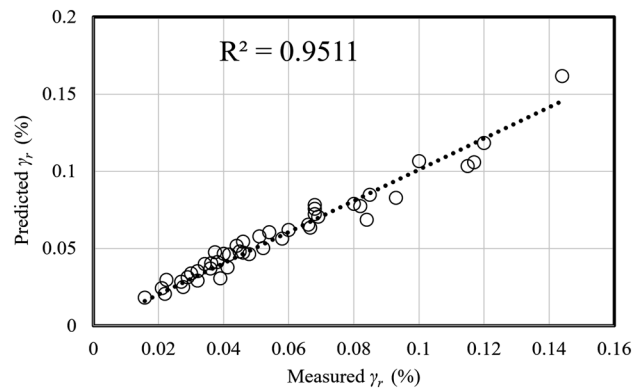
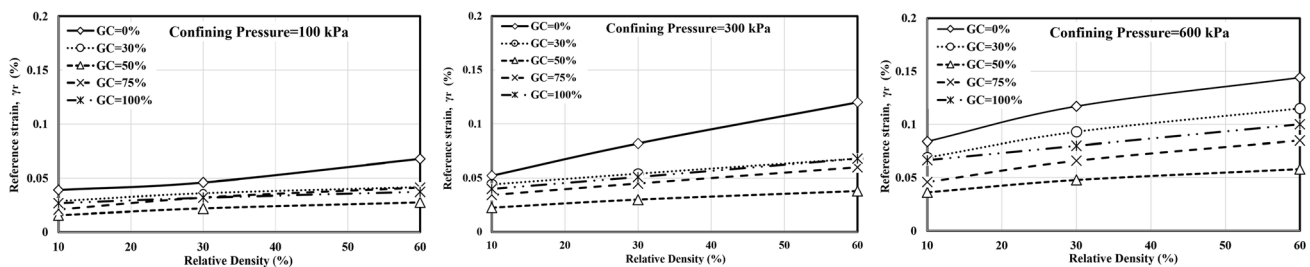**Fig. 18** Predicted versus measured values of γ_r

Fig. 17 Variation of reference strain, γ_r, with relative density for various confining pressures
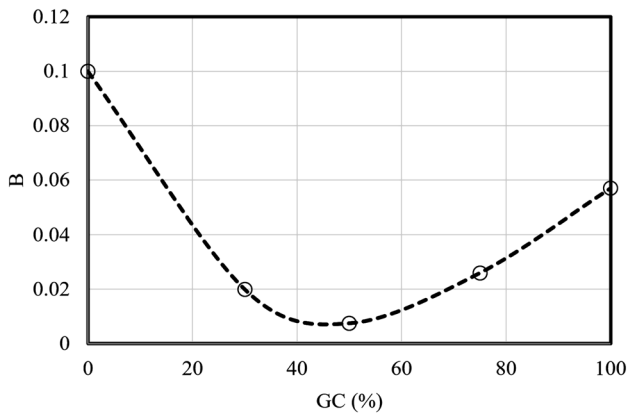
Fig. 19 Variation of *B* parameter as a function of gravel content

$$\frac{G}{G_{\max}} = \frac{1}{1 + \left(\frac{\gamma}{\gamma_{\text{ref}}}\right)}, \tag{8}$$

where G is the shear modulus corresponding to γ, $G_{\max}$ is the maximum shear modulus and γ_r is the reference shear strain value ($\gamma_r = \tau_{\max}/G_{\max}$).

Hardin and Drnevich [6] also proposed an approximate shape for the material damping curve as:

$$\frac{D}{D_{\max}} = \frac{\frac{\gamma}{\gamma_r}}{1 + \frac{\gamma}{\gamma_r}}, \tag{9}$$

where $D_{\max}$ is the maximum damping ratio that depends on soil type, confining pressure, number of cycles and loading frequency. Darendeli [49] presented a predictive modified hyperbolic model for estimating normalized shear modulus as:

$$\frac{G}{G_{\max}} = \frac{1}{1 + \left(\frac{\gamma}{\gamma_r}\right)^\alpha}, \tag{10}$$

where α is a curvature parameter to better fit the data corresponding to small and large strains and γ_r is the reference shear strain that controls the efficient normalization of shear strain. Increasing α increases the normalized stiffness at small shear strain amplitudes, but decreases the stiffness at large shear strain amplitudes.

For the material damping curve, Darendeli [49] used the normalized modulus reduction curve and Masing behaviour as a criterion with which to evaluate material damping. In the Darendeli method, the material damping curve is calculated by evaluating the hysteresis loops for a given modulus reduction curve assuming the validity of the Masing behaviour. Darendeli [49] introduced function F, that adjusts damping at high strains as:
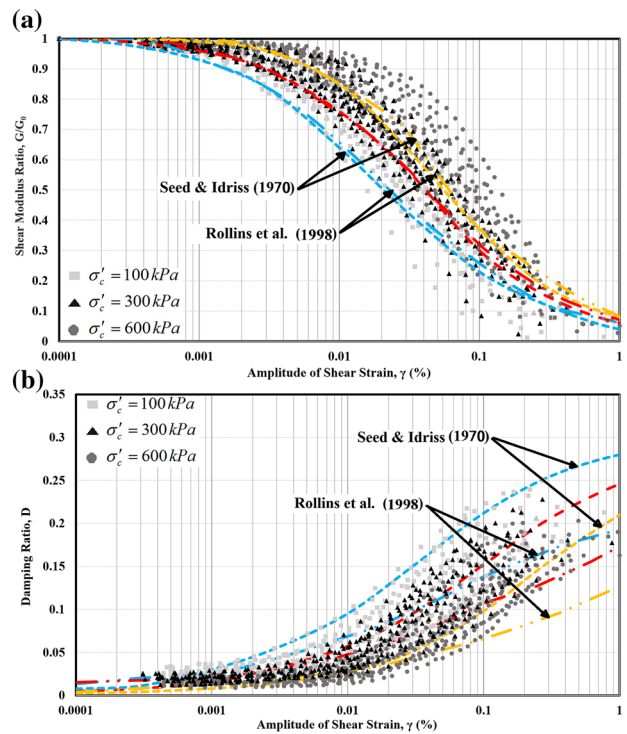

Fig. 20 Comparison of the tests results with recommended **a** $G/G_{\max}$–γ curves and **b** D–γ curves developed by Rollins et al. [35] and Seed and Idriss [19]

$$F = b \times \left[\frac{G}{G_{\max}}\right]^p, \tag{11}$$

where ($G/G_{\max}$) is the normalized modulus reduction curve and b and p are model parameters that control the characteristics of this function. Parameter p was replaced by a constant value of 0.1 to simplify the model [49].

According to Darendeli [49], the material damping curve is expressed as:

$$D = b \times \left[\frac{G}{G_{\max}}\right]^{0.1} \times D_{ma\sin g} + D_{\min}, \tag{12}$$

where $D_{\min}$ is the material damping ratio at small strains (in the linear range). Darendeli [49] used a four-parameter model (γ_r, a, b and $D_{\min}$) to characterize the normalized modulus reduction and material damping curves.

The shear modulus reduction data of all specimens with different gravel contents are plotted along with the upper, mean and lower curves of $G/G_{\max}$ as reported by Rollins et al. [35] and Seed and Idriss [19] in Fig. 20a. It is clear that the curves developed by Rollins et al. [35] and Seed and Idriss [19] underestimated the values of the normalized shear modulus at small-to-medium shear strain amplitudes and overestimated them at large shear strain amplitudes. It

appears that the G/G_{max}-γ curves developed by Rollins et al. [35] and Seed and Idriss [19] require modification, especially at small-to-medium shear strain amplitudes.

Comparison was also carried out of the D–γ data and the upper, mean and lower curves of D–γ as reported by Seed and Idriss [19] and Rollins et al. [35] in Fig. 20b. As seen, the damping ratios of the specimens at various gravel contents were within the range proposed by Seed and Idriss; however, the range proposed by Rollins et al. tended to underestimate the damping at large strain amplitudes. It appears that the D–γ curves developed by Seed and Idriss [19] provide good prediction of damping ratios in sand-gravel mixtures.

The best-fit functional relationship for the G/G_{max}–γ data based on confining pressure is shown in Fig. 21a as a modified hyperbolic equation in the form proposed by Darendeli [49]. Curve-fitting parameters (γ_r and α) of the mean, lower and upper bounds are presented in Table 2. As shown, curvature parameter α was a constant equal to 1.1 for all cases and the values of γ_r were determined based on the test data as a function of confining pressure and position of curve (lower, mean or upper curve). Figure 21a shows that the normalized shear modulus data fall within the ranges proposed by Darendeli with an appropriate choice of curve-fitting parameters. Figure 21b shows the D–γ data for the specimens along with the D–γ curves reported by Darendeli and indicates that

Table 2 Curve-fitting parameters (γ_r and α)

Confining pressure (kPa)	Position of curve	γ_r	α
100	Lower	0.07	1.1
	Mean	0.034	1.1
	Upper	0.015	1.1
300	Lower	0.1	1.1
	Mean	0.055	1.1
	Upper	0.02	1.1
600	Lower	0.15	1.1
	Mean	0.08	1.1
	Upper	0.03	1.1

the ranges proposed by Darendeli were not very sensitive to confining pressure variation, but the D–γ data exhibited greater sensitivity to it.

5 Conclusions

A series of bender element, resonant column and cyclic triaxial tests were carried out on fully-saturated specimens to investigate the dynamic properties of sand-gravel mixtures. Based on the results, the following conclusions could be drawn:

1. The normalized modulus reduction and material damping curves of the saturated sand-gravel mixtures were mainly affected by confining pressure, relative density, gravel content and cyclic strain amplitude. More specifically:

   (a) Pure sand experienced less normalized modulus reduction with an increase in strain than the sand-gravel mixture and pure gravel, while the sand-gravel mixture specimens with intermediate gravel contents displayed the greatest degradation of normalized modulus. The effects of gravel content (GC) on the stiffness degradation and damping ratio were based on the intergrain state concept.

   (b) Pure sand exhibited slightly lower damping values in comparison with the sand-gravel mixtures. At a given relative density and confining pressure, increasing the gravel content up to 50% slightly increased the damping values, which then decreased after 50%.

   (c) The relative density and confining pressure influenced the normalized modulus reduction and damping ratio, especially at large strains, such that an increase in confining pressure or relative den-
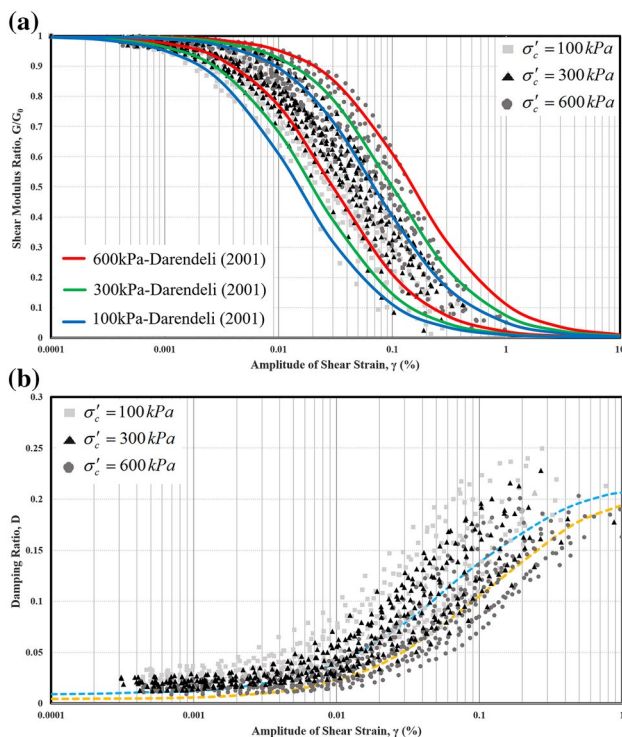

Fig. 21 Comparison of the tests results with recommended; **a** G/G_{max}–γ curves and **b** D–γ curves developed by Darendeli [49]

sity shifted the modulus reduction curves to the right and either upward (for G/G_{max}) or downward (for D).

2. The performance of the BE test was analysed by comparing the results with the RC test, which is renowned for the quality of its measurements based on G_{max}. The results of the tests indicated that the G_{max} obtained from these testing methods showed good agreement only for sand specimens which contained less than 75% gravel, while the results were different for specimens containing more than 75% gravel. The greatest difference between methods was for pure gravel specimens. The results indicate that the BE test did not perform as well for uniform gravelly soil and that the G_{max} obtained from BE testing was smaller than the maximum values of shear modulus obtained from RC testing. This may be because of the path through which the shear wave passes among the grains of gravel.

3. The BE tests results showed that the dimensions of the specimen should exceed wavelength λ by at least threefold ($D/\lambda \geq 3$) in order to avoid such dispersion. The results indicated that, in order to minimize the near-field effect, the value of d/λ should be greater than 3.

4. The G_{max} of the gravel-sand mixtures depends on relative density, confining pressure and gravel content. An increase in the confining pressure or relative density resulted in a nonlinear increase in G_{max} such that the effect of confining pressure was greater than that of relative density. In addition, pure sand exhibited significantly lower G_{max} values than the sand-gravel mixture or pure gravel. G_{max} increased nonlinearly with gravel content. This continued until a maximum value of G_{max} was reached at a gravel content of 50%.

5. The shear strain amplitude at which $G/G_{max} = 0.5$ (γ_r) increased with an increase in confining pressure or relative density. The confining pressure was more effective than relative density in this case. Also, the γ_r of the pure sand was greater than that for the sand-gravel mixtures at a given confining pressure and relative density. The results indicate that the values of γ_r can be predicted as function of relative density (or void ratio), confining pressure and gravel content.

6. In the current study, validation of the previous model and empirical curves was carried out using tests results.

   (a) According to the results, the G/G_{max}–γ curves developed by Rollins et al. [35] and Seed and Idriss [19] underestimated the values of G/G_{max} at small-to-medium shear strain amplitudes and overestimated the values of G/G_{max} at large strain amplitudes. The results indicate that the D–γ ranges proposed by Rollins et al. require modification for large strain amplitudes; however, the D–γ curves proposed by Seed and Idriss showed reasonably good performance for all tests results.

   (b) The results indicated that the values of G/G_{max} fell within the ranges proposed by Darendeli [49] with the appropriate choice of curve-fitting parameters. In addition, the D–γ ranges proposed by Darendeli were validated by the tests results. These results indicate that the D–γ ranges proposed by Darendeli require modification in order to increase sensitivity to confining pressure variation.

References

1. Humar JL (2002) Dynamics of structures. Taylor & Francis, London
2. ASTM (2016) Modulus and damping of soils by fixed-base resonant column devices ASTM D4015–15. ASTM 1–22. https://doi.org/10.1520/D4015-15
3. ASTM (2016) Standard test methods for the determination of the modulus and damping properties of soils using the cyclic triaxial apparatus 1. ASTM. https://doi.org/10.1520/D3999-11E01.1.6
4. Atkinson JH, Coop MR, Stallebrass SE, Viggiani G (1993) Measurement of stiffness of soils and weak rocks in laboratory tests. In: Proc. 26th Conf. Eng. Grp. Geol. Soc. Leeds, Cripps al. (eds), Balkema Rotterdam Eng. Geol. Gr. pp 21–27
5. Seed HB, Idriss IMM (1982) Ground motions and soil liquefaction during earthquakes , vol 5. Earthquake Engineering Research Institute
6. Hardin BO, Drnevich V (1973) Shear modulus and damping in soils: measurement and parameter effects. J Terramechanics 9:102. https://doi.org/10.1016/0022-4898(73)90212-7
7. Ni S (1988) Dynamic properties of sand under true triaxial stress states from resonant/column torsional shear tests
8. Seed HB, Wong RT, Idriss IM, Tokimatsu K (1986) Moduli and damping factors for dynamic analyses of cohesionless soils. J Geotech Eng 112:1016–1032. https://doi.org/10.1061/(ASCE)0733-9410(1986)112:11(1016)
9. Stokoe KH, Darendeli MB, Andrus RD, Brown LT (1999) Dynamic soil properties: Laboratory, field and correlation studies. In: Earthq Geotech Eng Proc 2nd Int Conf Earthq Geotech Eng Lisbon, June 1999 (3 vol), pp 811–845
10. Zhang J, Andrus RD, Juang CH (2005) Normalized shear modulus and material damping ratio relationships. J Geotech Geoenvironmental Eng 131:453–464. https://doi.org/10.1061/(ASCE)1090-0241(2005)131:4(453)
11. Vucetic M, Dobry R (1991) Effect of soil plasticity on cyclic response. J Geotech Eng 117:89–107. https://doi.org/10.1061/(ASCE)0733-9410(1991)117:1(89)
12. Wang ZJ, Luo YS, Guo H, Tian H (2012) Effects of initial deviatoric stress ratios on dynamic shear modulus and damping ratio of undisturbed loess in China. Eng Geol 143–144:43–50. https://doi.org/10.1016/j.enggeo.2012.06.009
13. Wichtmann T, Navarrete Hernández MA, Triantafyllidis T (2015) On the influence of a non-cohesive fines content on small strain stiffness, modulus degradation and damping of quartz sand. Soil Dyn Earthq Eng 69:103–114. https://doi.org/10.1016/j.soildyn.2014.10.017

14. Mir Mohammad Hosseini SM, Hajimohammadi AA, Hajimohammadi AR (2010) The validity assesment of laboratory shear modolus using in-situ seismic piezocone test results. Int J Civ Eng 8:134–142

15. Hardin B (1973) Shear modulus of gravel, Report-TR74–73-CE19

16. Tanaka Y, Kudo K, Yoshida Y, Ikemi M (1987) A study on the mechanical properties of sandy gravel—dynamic properties of reconstituted sample. Central Research Institute of Electric Power Industry. Report U, 87019

17. Lin S-Y, Lin PS, Luo H-S, Juang CH (2000) Shear modulus and damping ratio characteristics of gravelly deposits. Can Geotech J 37:638–651. https://doi.org/10.1139/cgj-37-3-638

18. Liao T, Massoudi N, McHood M, Stokoe KH, Jung MJ, Menq FY (2013) Normalized shear modulus of compacted gravel. In: Proc. 18th Int. Conf. Soil Mech. Geotech. Eng. Paris, pp 1535–1538

19. Seed HB, Idriss IM (1970) Soil moduli and damping factors for dynamic response analyses. Report No. EERC 70–10, Earthquake Engineering Research Center, University of California, Berkeley, p 40

20. Gu X, Yang J (2011) Laboratory measurement of shear stiffness of decomposed granite. In: 15th Eur. Conf. Soil Mech. Geotech. Eng. IOS Press, pp 191–196

21. Hardin BO, Black WL (1967) Sand stiffness under various triaxial stresses. J Terramechanics 4:70. https://doi.org/10.1016/0022-4898(67)90133-4

22. Hassanipour A, Shafiee A, Jafari MK (2011) Low-amplitude dynamic properties for compacted sand-clay mixtures. Int J Civ Eng 9:255–264

23. ASTM (2013) ASTM D4253–00: standard test methods for maximum index density and unit weight of soils using a vibratory table. ASTM Stand. https://doi.org/10.1520/D4253-00R06

24. ASTM (2006) ASTM D4254–00: standard test methods for minimum index density and unit weight of soils and calculation of relative density. ASTM Stand I:9. https://doi.org/10.1520/D4254-00R06E01.1.3

25. Evans MD, Zhou S (1995) Liquefaction Behavior of Sand-Gravel Composites. J Geotech Eng 121:287–298. https://doi.org/10.1061/(ASCE)0733-9410(1995)121:3(287)

26. Yamamuro JA, Wood FM (2004) Effect of depositional method on the undrained behavior and microstructure of sand with silt. Soil Dyn Earthq Eng 24:751–760. https://doi.org/10.1016/j.soildyn.2004.06.004

27. Frost JD, Park JY (2003) A critical assessment of the moist tamping technique. Geotech Test J 26:57–70. https://doi.org/10.1520/GTJ11108J

28. Maleki M, Bayat M (2012) Experimental evaluation of mechanical behavior of unsaturated silty sand under constant water content condition. Eng Geol 141–142:45–56. https://doi.org/10.1016/j.enggeo.2012.04.014

29. Borhani A, Fakharian K (2016) Effect of particle shape on dilative behavior and stress path characteristics of chamkhaleh sand in undrained triaxial tests. Int J Civ Eng 14:197–208. https://doi.org/10.1007/s40999-016-0048-8

30. Selig E, Ladd R (1978) Preparing test specimens using undercompaction. Geotech Test J 1:16. https://doi.org/10.1520/GTJ10364J

31. Fakharian K, Eghbali A (2012) Effect of cyclic stress path in cement-treated sands using triaxial and simple shear tests. The twenty-second international offshore and polar engineering conference, International Society of Offshore and Polar Engineers, Rhodes, Greece, 17–22 June 2012

32. ASTM International (2011) D 4767–11. Standard test method for consolidated undrained triaxial compression test for cohesive soils. Annu B ASTM Stand 4:14. https://doi.org/10.1520/D4767-11

33. ASTM D 5311 (2013) Standard tests methods for load controlled cyclic triaxial strength of soil. ASTM, pp 1–11. https://doi.org/10.1520/D5311_D5311M

34. Aghaei Araei A, Reza Razeghi H, Hashemi Tabatabaei S, Ghalandarzadeh A (2012) Loading frequency effect on stiffness, damping and cyclic strength of modeled rockfill materials. Soil Dyn Earthq Eng 33:1–18. https://doi.org/10.1016/j.soildyn.2011.05.009

35. Rollins KM, Evans MD, Diehl NB III, William DD (1998) Shear modulus and damping relationships for gravels. J Geotech Geoenvironmental Eng 124:396–405. https://doi.org/10.1061/(ASCE)1090-0241(1998)124:5(396)

36. Jardine RJ, Symes NJ, Burland JB (1985) Discussion: the measurement of soil stiffness in the triaxial apparatus. Géotechnique 35:378–382. https://doi.org/10.1680/geot.1985.35.3.378

37. Senetakis K, Anastasiadis A, Pitilakis K (2015) A comparison of material damping measurements in resonant column using the steady-state and free-vibration decay methods. Soil Dyn Earthq Eng 74:10–13. https://doi.org/10.1016/j.soildyn.2015.03.009

38. Hwang SK (1997) Investigation of the Dynamic Properties of Natural Soils. PhD Dissertation U of T at A 394

39. Huot FG, Vulliet L (1998) Small strain elastic moduli of a saturated sand. In: Biot conference on poromechanics. Louvain-La-Neuve, September 1998 (No. LMS-CONF-2006-017), pp 245–251

40. Seed RB, Cetin KO, Moss RES (2001) Recent advances in soil liquefaction engineering and seismic site response evaluation. In: Fourth Int. Conf. Recent Adv. Geotech. Earthq. Eng. Soil Dyn. Symp. Honor Profr. W.D. Liam Finn. pp 1–45

41. Lashkari A (2016) Prediction of flow liquefaction instability of clean and silty sands. Acta Geotech 11:987–1014. https://doi.org/10.1007/s11440-015-0413-9

42. Dyvik R, Madshus C (1985) Lab measurements of G_{max} using Bender elements. In: Advances in the art of testing soils under cyclic conditions. ASCE, pp 186–196

43. Fam MA, Cascante G, Dusseault MB (2002) Large and small strain properties of sands subjected to local void increase. J Geotech Geoenvironmental Eng 128:1018–1025. https://doi.org/10.1061/(ASCE)1090-0241(2002)128:12(1018)

44. Hoyos LR, Suescún-Florez EA, Puppala AJ (2015) Stiffness of intermediate unsaturated soil from simultaneous suction-controlled resonant column and bender element testing. Eng Geol 188:10–28. https://doi.org/10.1016/j.enggeo.2015.01.014

45. Leong EC, Yeo SH, Rahardjo H (2005) Measuring shear wave velocity using bender elements. Geotech Test J 28:488–498. https://doi.org/10.1520/GTJ12196

46. Liu X, Yang J, Wang G, Chen L (2016) Small-strain shear modulus of volcanic granular soil: An experimental investigation. Soil Dyn Earthq Eng 86:15–24. https://doi.org/10.1016/j.soildyn.2016.04.005

47. Yunmin C, Han K, Ren-Peng C (2005) Correlation of shear wave velocity with liquefaction resistance based on laboratory tests. Soil Dyn Earthq Eng 25:461–469. https://doi.org/10.1016/j.soildyn.2005.03.003

48. RaviShankar BV (Department of CEIB, Sitharam TG (Department of CEIB, Govindaraju L (Department of CEIB) (2005) Dynamic properties of Ahmedabad sands at large strains. IGC, Ahmedabad 17–19 December 369–372

49. Darendeli MB (2001) Development of a new family of normalized modulus. CEUR Workshop Proc. https://doi.org/10.1017/CBO9781107415324.004